Restoration of Corrupted Optical Fuyo-1 (JERS-1) Data Using Frequency Domain Techniques

C.R. de Souza Filho, S.A. Drury, A.M. Denniss, R.W.T. Carlton, and D.A. Rothery

Abstract

The image data collected by Fuyo-1's sensors covering the visible and the short wave infrared (SWIR) are affected by severe noise problems. The important narrow SWIR channels show the worst defects. Artifacts originally introduced by the satellite sensors (unprocessed Level 0 data) were exaggerated by the Earth-rotation correction applied by NASDA (Level 2 data). Fourier analysis is used to characterize these artifacts in the frequency domain. A scene-dependent Fourier operator that is able to eliminate the major noise components is described. This involves the construction of a binary mask derived from the difference between the Fourier spectra of two channels containing noise signals at similar frequencies and amplitude. This mask is used to modulate frequency domain images, so removing all noise components while preserving real image data with minimum loss and distortion in the spatial domain. Fuyo-1 brightness saturation problems can also be minimized by applying a Gaussian contrast stretch to the Fourier spectra prior to image inversion. Based on our initial results using the recovery methods proposed here, we foresee an exciting new use for the thousands of seven-channel images already acquired by Fuyo-1.

Introduction

The Japanese Earth Resources Satellite (JERS-1, now renamed Fuyo-1) was launched into a 568-km, sun-synchronous orbit (97.7° inclination) by the National Space Development Agency (NASDA) of Japan on 12 February 1992. The orbital and optical design of Fuyo-1 allows a revisit period of 44 days. Fuyo-1 carries a synthetic-aperture radar (SAR) and an optical sensor (OPS) (anon., 1990; anon., 1991; Nishidai, 1993a; Nishidai, 1993b). Descending overpasses are between 10:30 and 11:00 AM local solar time. Images are acquired approximately one hour later than by Landsat-5, which causes a noticeable reduction in the length of solar shadows from topographic features and the suppression of some spatial detail.

The OPS package has two optical-electronic subsystems covering visible/near-infrared (VNIR), and short-wave infrared (SWIR) wavelengths. Both of these use linear CCD arrays (4096 elements) which act as pushbroom imaging devices. The SWIR array captures radiance from four wavebands in nadir mode (OPS 5: 1.60 to 1.71 μm, OPS 6: 2.01 to 2.12 μm, OPS 7: 2.13 to 2.25 μm, and OPS 8: 2.27 to 2.40 μm), while the VNIR arrays have a nadir mode for the first three channels (OPS 1: 0.52 to 0.60 μm, OPS 2: 0.63 to 0.69 μm, and OPS 3: 0.76 to 0.86 μm) and a forward-pointing mode (15.33° from nadir) for the very-near infrared channel (OPS 4: 0.76 to 0.86 μm) (Figure 1). OPS Channels 3 and 4 can therefore be used to obtain along-track stereoscopic coverage. The 32.2 μrad instantaneous field of view is expressed for each radiance signal as a 25.4-m (along-track) by 18.3-m (across-track) ground resolution cell in the unprocessed Level-0 data. Level-2 preprocessing corrects OPS scenes for Earth rotation and resamples data to 18-m-square pixels in parallelogram-shaped scenes covering approximately 75 by 75 km (4201 lines, 4680 samples, including border fill). Radiometric precision is at 6 bits (64 radiance levels).

The increased spatial resolution, along with the increased number of channels at shorter wavelengths, should mean that the Fuyo-1 OPS radiometer is capable of producing the most geologically significant data available from any current satellite platforms (Yamaguchi, 1987; Yamaguchi, 1988; Yamaguchi *et al.*, 1992, Nishidai, 1993a; Nishidai, 1993b). It was originally anticipated that the 6-bit OPS radiometric precision would cause some problems with image quality, because of the narrow dynamic range. It is now apparent that the main problems have come from unexpected on-board electronic fluctuations and failures which have caused severe noise degradation of the image data. All reported images collected by the satellite (Nishidai, 1993a; Ono, 1993), including those analyzed during this research, are affected to varying degrees by several noise structures, with the SWIR channels containing the worst defects. The noise component introduced during image capture is severe enough to jeopardize the effective use of Fuyo-1 data in all applications.

Geological Implications of Fuyo-1 Optical Data

The 2.0- to 2.5-μm atmospheric window is of great importance in geological remote sensing because it includes mineralogically diagnostic absorption features. Sharp absorption features commonly found around the 2.2-μm (Figure 2) region are characteristic of an additive combination of the Al-OH fundamental bend with the OH^- fundamental stretch. Dioctahedral layer-silicates have such molecular combinations (Hunt, 1980). Differences in the OH^- sites with the Al-OH fundamental produce intense absorption features that shift systematically between 2.16 and 2.23 μm (Hunt, 1980) and also vary in shape. For example, absorption features around 2.2 μm are sharp for pyrophyllite, broad for montmorillonite and muscovite, or multiple as in kaolinite and dickite (Hunt and Ashley, 1979; Hunt, 1981). Common absorption

Department of Earth Sciences, The Open University, Walton Hall, Milton Keynes, MK7 6AA, United Kingdom.
C.R. de Souza Filho is currently with the Instituto de Geociencias, University of Campinas, P.O. Box 6152, CEP 13081-970, Campinas, São Paulo, Brazil.

Photogrammetric Engineering & Remote Sensing, Vol. 62, No. 9, September 1996, pp. 1037–1047.

0099-1112/96/6209-1037$3.00/0

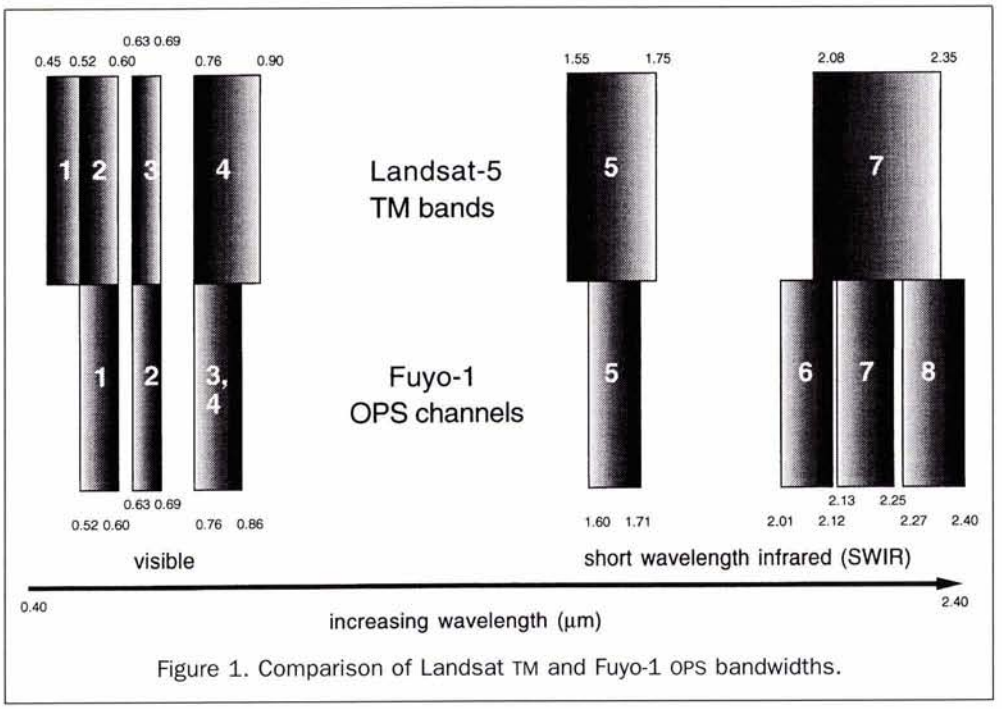

Figure 1. Comparison of Landsat TM and Fuyo-1 OPS bandwidths.

features found around 2.3 μm, with an absence of 2.2-μm absorptions, are attributed to the presence of the OH^- stretch plus the Mg-OH bend fundamentals, characteristic of the trioctahedral minerals and also Mg-bearing amphiboles (Hunt and Ashley, 1979). For example, epidote, chlorite, tremolite-actinolite, talc, and serpentine have diagnostic multiple absorption features in and around the 2.3-μm region (Figure 2). Carbonate minerals also exhibit absorptions around 2.35 μm (Figure 2), which are considered as overtones of one of the five fundamental vibrations of the CO^{3-} radical (Hunt and Salisbury, 1970). These overtones and combination tones of the various CO^{3-} fundamentals produce additional absorption features at 1.9, 2.0, and 2.15 μm.

The Fuyo-1 SWIR channels (OPS 6, 7, and 8) cover the atmospheric window ranging from 2.0 to 2.40 μm (Figure 1). Landsat TM records just one broad channel from this part of the spectrum (TM 7; 2.08 to 2.35 μm), while Fuyo-1 records three narrow independent channels, which in total cover a slightly larger window than TM 7 (Figure 1). Fuyo-1's sensors can, therefore, potentially detect the wavelength shift of an absorption feature as it shifts from one channel to another, where the TM would be incapable of detecting any change. This capability means that many rock-forming minerals can be distinguished from their distinct spectral responses in these individual channels. It is, thus, vital to render the Fuyo-1 SWIR data free from noise, because of their potential use in geological mapping and mineral exploration.

The objectives of this paper are (1) to provide a detailed characterization of Fuyo-1 OPS image defects in both raw Level-0 data, and in pre-processed Level-2 data that are being distributed by NASDA; (2) to discuss the limitations of known filtering techniques in minimizing Fuyo-1 OPS image defects; and (3) to develop a new frequency filtering technique which reduces Fuyo-1 noise and, optionally, brightness saturation effects, with minimum loss and distortion of important spatial data. We show that, although severely corrupted, Fuyo-1 images are not beyond recovery. We evaluated the noise content and the efficiency of this new recovery technique using several Fuyo-1 scenes from Libya, Eritrea, Oman, and Chile. Here, we use examples from Eritrea and Oman by way of illustration.

Defects in Fuyo-1 OPS Data

Defects associated with Fuyo-1 OPS data have a very systematic and specific nature. Some noise structures are related to real features in the scene, and distinction between the two in the spatial domain is difficult (Figures 3a, 3b, and 3c). As a result, convolution filters are unable to eliminate or selectively reduce unwanted noise artifacts while preserving important image data. In the spatial domain, Principal Component Analysis (PCA) can be used to reduce noise, relying on the principle that noise structures are poorly correlated between channels (Schowengerdt, 1983; Rothery and Hunt, 1990). PCA transforms the data so that the noise component is cast into one or more of the high-order principal components. Using this technique on Fuyo-1 data confined some noise in the higher order PCs, but a significant amount of residual noise was present in the low-order components, making the results of this method unsatisfactory.

For these reasons, analysis of Fuyo-1 artifacts in the frequency domain and filtering using Fast Fourier Transforms (FFTs) is the most suitable technique to attempt image restoration. Details of the theoretical basis and applications of Fourier Transforms are discussed widely in image processing literature (e.g., Gonzalez and Wintz, 1977; Castleman, 1979; Schowengerdt, 1983; Niblack, 1986; Jain, 1989; Marion, 1991). The OPS image defects are described and analyzed below in terms of both their spatial and frequency domain features.

Spatial Domain Features

The following sections present major spatial domain artifacts observed in the unprocessed (Level-0) and Earth-rotation corrected (Level-2) data.

Level-0 Data

An example of unprocessed Level-0 Fuyo-1 OPS data, captured early in the satellite's history over Libya (Figure 3a), reveals a number of important defects in the raw data. Aside from the along- and across-track defects, which are common in all images from pushbroom systems (caused by the slightly different responses of individual CCDs in the imaging array), fluctua-

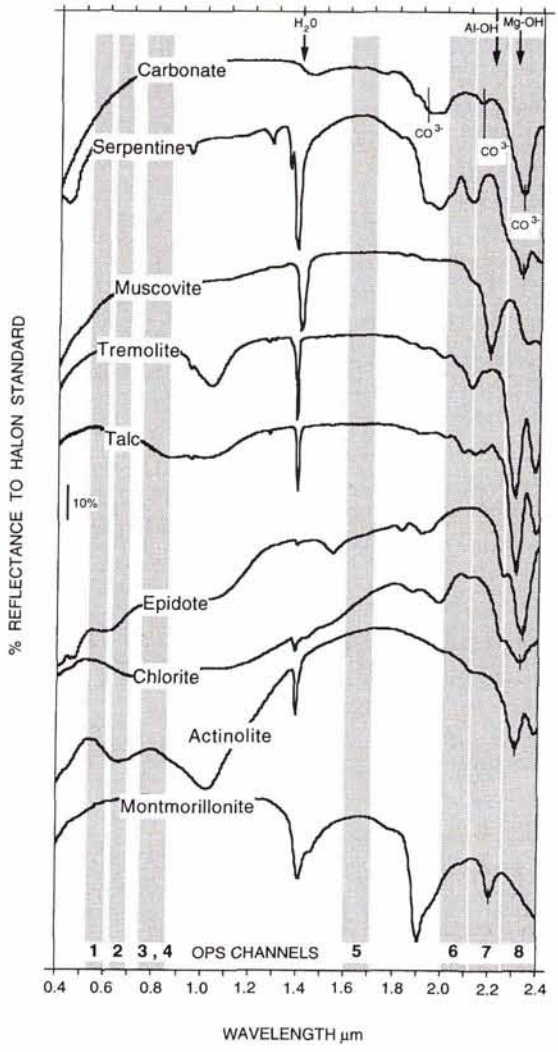

Figure 2. OPS channels bandwidth and their relation to the absorption features of common rock and ore forming minerals (spectra extracted from Grove *et al.* (1992)).

tions in the system electronics and or instability of the power supply have introduced other serious noise structures (Ono, 1993; Shimada, 1993; Tanaka and Shimada, 1993). The Level-0 VNIR channels are relatively free of system defects, with the exception of across-track striping and low dynamic ranges. This noise has a simple structure and is comprised of irregular horizontal lines, visually similar to Landsat MSS horizontal striping. This striping occurs to some degree in all VNIR channels regardless of gain setting, although at high gain modes it seems to increase (Ono, 1993; Shimada, 1993).

Level-0 SWIR data are plagued by systematic problems. In the Libyan image provided by NASDA, the dynamic ranges of all SWIR channels are as low as the VNIR channels, sometimes occupying less than ten radiance levels within the 6-bit range. The same is reported by Nishidai (1993b) over a great number of scenes and is admitted to be a result of improper gain settings . Misregistration is also a problem, both between individual SWIR channels and between the SWIR and VNIR channels. The across-track striping in the SWIR channels is similar to that found in the VNIR channels; Channel 8 usually being the worst (see Figure 4a[1]). The along-track striping has a complex structure, being made up of vertical alternating columns, one sample wide, of either relatively high or low radiances (Figures 4a[1] and 4a[2]). These columns are of variable length, and the "polarity" seems to switch along the columns. Related to this problem is irregular along-track disarray of signals from surface features which trend across-track, for example, drainage channels. These introduce a "blurring" into the images parallel to the satellite flight direction. This is similar in appearance to motion blur. This "image blur" is particularly obtrusive in Channels 6 and 7, but also affects Channels 5 and 8. According to Nishidai (1993a; 1993b), the "image-blur" defect is linked to the failure of individual charge couple devices (CCDs) to respond to different ranges of radiance encountered at boundaries between distinct features (i.e., it is associated with edges). The noise produced by this system defect is therefore scene dependent and, as we shall show, can only be dealt with using procedures derived from each affected scene, not by standard approaches.

Level-2 Data

Level-2 Fuyo-1 data is corrected by NASDA for Earth rotation, and for band misregistration. Removal of the noise component is not undertaken during this preprocessing.

Our preliminary analysis shows larger registration errors between the VNIR and SWIR channels than those reported by Shimada (1993) for Level-2 data. Being misregistered from 1 up to 6 pixels in both along- and across-track directions, VNIR and SWIR Level-2 images still require some geometric rectification before being combined together as false color composites.

The Earth rotation correction applied by NASDA exaggerates the along-track noise seen in the Level-0 data. Its appearance in Level-2 data is very distinct across all VNIR and SWIR channels. This is because the algorithm used for the Earth rotation correction dislocated the "blurring" into small fragments, turning the Level-0 vertically positioned defects (linked with even and odd detector failures) into broad diagonal noise patterns in the Level-2 data at about 20° clockwise to the across-track direction. Figure 4b[2] shows the detailed structure of these diagonal noise patterns. The diagonal striping is a function of the original along-track striping and blurring, and its obtrusiveness increases proportionally with the severity of the original defects in the raw image (Kazuya Okada, pers. comm.). The horizontal noise which appears on the Level-0 data (in all VNIR and SWIR channels) has not been significantly affected by the algorithm. This noise has not been rotated, just translated in a horizontal direction (Figure 4b[1]). Overall, Level-2 SWIR Channels 5 and 8 are less severely degraded by noise structures than are Channels 6 and 7. In all but one case, we found SWIR Channel 7 to be the most severely affected by noise.

Frequency Domain Features

Figures 5a and 5b show actual and schematic magnitude plots, respectively, obtained from the Level-0 and Level-2 OPS SWIR images pictured in Figures 3a and 3b. The FFT axes are the "wrong" way around when compared with conventional expression (see Gonzalez and Wintz, 1977; Schowengerdt, 1983, Hummer-Miller, 1990), but this is an arbitrary convention. With this arrangement, the process runs at maximum speed. The Fourier Transform displays complex, though systematic, structures, which are difficult to explain without a detailed knowledge of the defects introduced during image capture and the methods involved in preprocessing. The broad clusters in the magnitude plot represent real scene attributes in the original image. In this case, the clusters composing the region around the zero relative frequency point (center of plots in Figures 5a[1], 5a[2], 5b[1], and 5b[2]) can be taken to represent the majority of the spatial frequency distri-

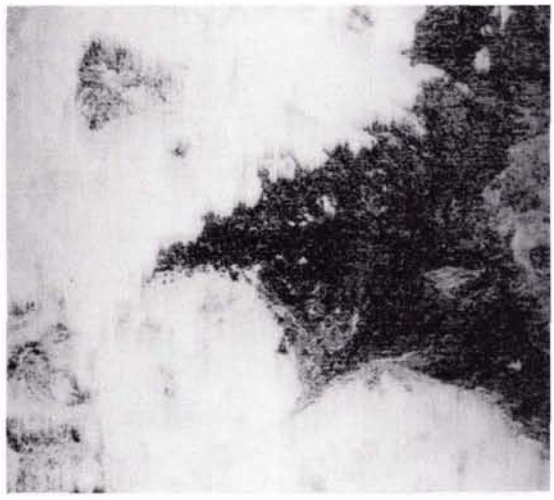

(a)

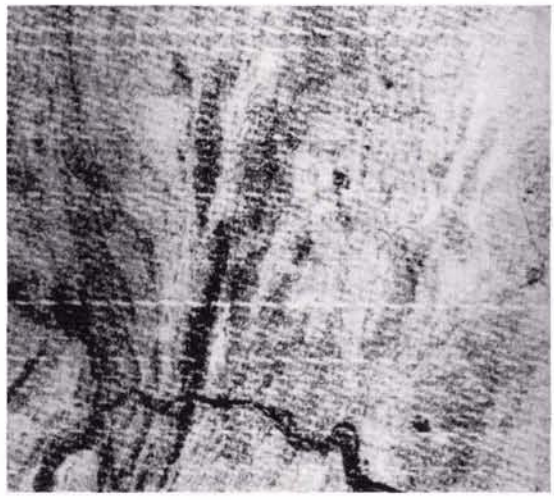

(b)

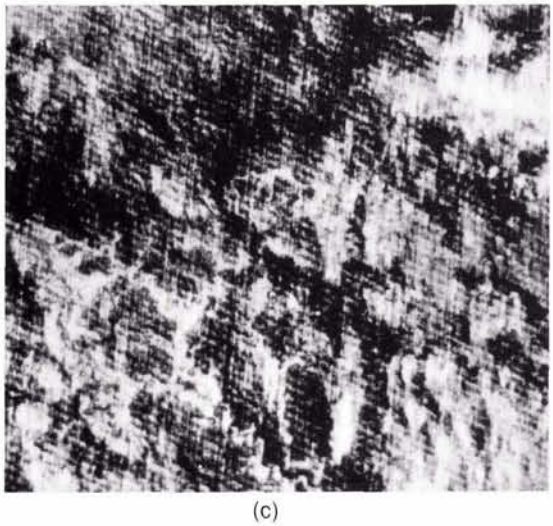

(c)

Figure 3. Examples of Fuyo-1 OPS data (1024 by 1024 sub-scenes). (a) Level-0 Channel-8 data of northern Libya. (b) Level-2 Channel-8 data of northern Eritrea. (c) Level-2 Channel-6 data of the Maqsad region, Oman. Each shows noise resulting from across- and along-track defects (a simple texture filter was applied to all images to picture the noise more distinctively). The various noise structures are discussed in the text and illustrated in more detail by Figure 4.

bution resulting from real topographic and geological features in the image. The shape and width of this region indicates an almost random range of directional attributes and sizes of the real image features. Conversely, the noise components of these plots show a striking degree of order.

The magnitude plots of Level-0 images (Figures $5a^1$ and $5a^2$) exhibit sets of horizontal and vertical spots aligned through the origin. Spots along the horizontal lines A-A', A_1-A_1', and A_2-A_2' (other, more faint, spots are also present) signify the major horizontal defects in the original image (i.e., the across-track horizontal striping). The consistent periodicity of this noise in the spatial domain is expressed as a series of well-defined spikes in the magnitude plots, representing energy concentrations at isolated spatial frequencies. These spikes comprise bright spots with varying intensities (variable amplitude) from low to high frequencies. In Level-2 magnitude images (Figures $5b^1$ and $5b^2$), horizontal noise is similar to that of the Level-0 data (C-C', C_1-C_1', C_2-C_2').

The vertically aligned spikes in Figures $5a^1$ and $5a^2$ (line B-B') express the along-track, vertical blurring in Level-0 images. In the frequency domain, the structure of this noise appears similar to the horizontal striping but differs as regards the nature of the spikes. These spikes are, in detail, star-like clusters on the magnitude plots and not individual spots as with the horizontal noise. The star-like clusters are not single frequency bursts, but have broad "skirts," which contain information about artificial interference patterns in the image itself (Figure $4a^2$). This property is clearly visible on the original magnitude plots of the SWIR channels, where the broader clusters are observed at high frequencies. In addition to this, the noise varies from very high frequencies to very low frequencies. This often makes noise nearly indistinguishable from the real image data even in the magnitude plot and therefore practically impossible to remove by convolution filters in the spatial domain.

The FFTs for Level-2 images (Figures $5b^1$ and $5b^2$) also show a much more complex structure for along-track noise due to the Earth rotation correction pre-processing. Here, Level-0 noise structures have been rotated out of vertical orientation (line D-D'), and the star-like clusters indicating the location of the noise have been enlarged. The pre-processing has also created a less prominent twin set of sub-vertically aligned high frequency clusters (e.g. line E-E' and F-F'), which are parallel to the main line (D-D'). These two lines do not cross the origin and are a peculiar feature seen in the magnitude plots extracted from Level-2 SWIR channels only. They probably correspond to aliased noise components. The change in the defect's directionality in Level-2 data can be understood in the light of the rotation property of the Fourier Transform (Gonzalez and Wintz, 1977).

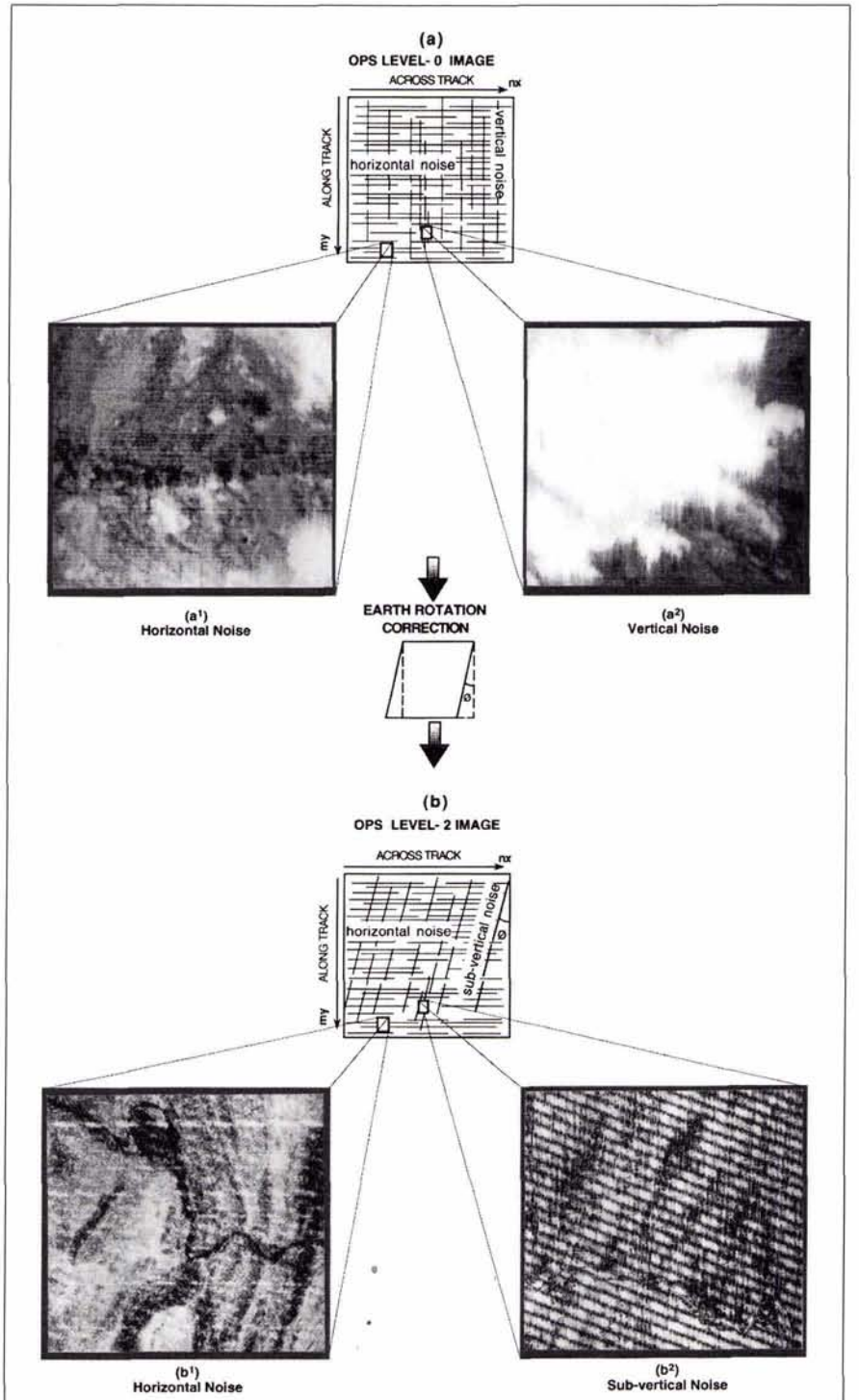

Figure 4. Noise features observed in Level-0 and Level-2 SWIR data in the spatial domain. (a) Shows noise in Level-0 data (see Figure 3a) diagrammatically (a^1 and a^2 show enlargements of the actual noise due to across- and along-track defects). (b) Shows how the Earth-rotation correction modifies the appearance of noise in Level-2 data (see Figure 3b) (b^1 and b^2 show enlargements of the Level-2 noise components).

Despite the apparently bewildering variety of systematic features seen in the magnitude plots of the Level 2 data, they probably all have quite simple origins related directly to primary sensor failures. Many have resulted from the generation of artifacts by "interference" between the original OPS defects in the Level-0 data and the preprocessing algorithms involved in Earth rotation correction. We shall now look at methods which can be applied to isolate and remove the majority of these noise structures from Level-2 data, thereby rendering the data more useful in various applications.

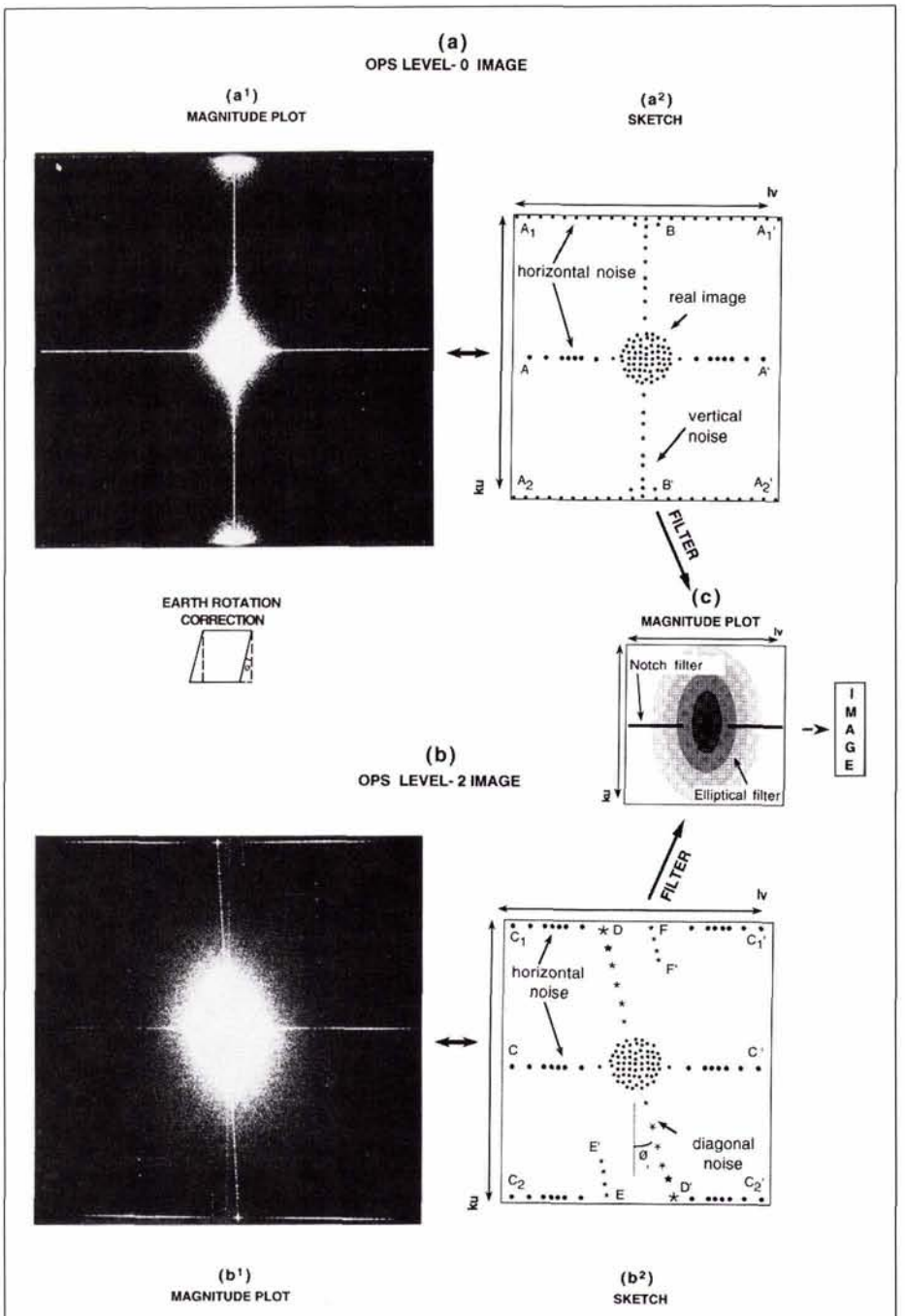

Figure 5. Magnitude plots of Level-0 (a) and Level-2 (b) noise-corrupted Fuyo-1 image data (Figure 3a and 3b) as images (a^1, b^1) and explanatory sketches (a^2, b^2). Note that there is no distinction between the grey levels representing the noise signal (star-like clusters) from those representing the image signal at and around the zero-frequency point. (c) Schematic diagram of conventional Fourier filters.

Image Restoration and Noise Removal

Matsunaga *et al.* (1993 and pers. comm.) developed a method to reduce the perceived blurring effects in the OPS SWIR data by modeling the CCDs response delays. Although the technique allows noise to be suppressed to some extent, the restored images show remaining artifacts and poor quality. We tried traditional methods of dealing with noise reduction using convolution filters (C.R. de Souza Filho, unpublished data), including the ones proposed by Crippen *et al.* (1994 and pers. comm.) for the Fuyo-1 data, all with unsatisfactory results. Experiments exploiting the potential of Fourier Transform functions to isolate noise have proved more successful.

Conventional Fourier Operators

Noise filtering in the frequency domain involves designing masks that remove aberrant features from the Fast Fourier Transform (FFT), and then applying the Inverse Fourier Transform (IFT) to recreate the restored image in the spatial domain.

Notch Filters

The simplest frequency domain filter multiplies the FFT by a zero-weighted mask, whose shape exactly fits or totally encompasses the aberrant feature. This is a "notch filter" (Gonzalez and Wintz, 1977). All other values of the transform outside the mask are multiplied by one (i.e., a binary mask). If the interference pattern representing the spatial noise structures has a periodic nature, producing bursts of concentrated energy along the FFT axes, and if these bursts are at a sufficient distance from the image origin (i.e., at relatively high frequencies), they can be removed selectively by simply applying a notch filter. The across-track horizontal noise described before displays most of these characteristics, and can be eliminated completely using such a simple filter without causing the loss of important image information. The main drawback of this method is that an incorrect filtering is likely to add more noise to the image. The size and shape of the notch filter must be carefully designed to avoid the introduction of spurious patterns, such as ringing. This requires determining over how large a neighborhood the mask should be applied. Because it can be implemented easily, the use of notch filters should be strongly considered for those willing to work with Fuyo-1 VNIR channels, which are mostly affected by horizontal mid- to high-frequency noise. Figure 5c graphically shows how this sort of notch filter would be applied in the frequency domain.

For complex noise structures like those represented by the along-track striping, the use of notch filters may remove too much of the real image information. It is also necessary to remember that the star-like components related to this noise have broad skirts, containing information about the interference pattern, which are difficult to separate from the normal image background. Because several bursts are present, designing traditional notch filters can be tedious and non-effective, unless the filter parameters could be chosen with extreme accuracy.

Elliptically Symmetrical Fourier Filters

Another approach is to combine the Fourier Transform multiplicatively with a circular or elliptical filter that is symmetrical about the zero frequency point. The weighting of such filters varies from one at the origin to zero at high frequencies, according to some predetermined function. These filters therefore progressively mute or remove artifacts at high frequencies. Real image information dominates the spectrum at the low frequencies, and usually fades with increasing frequency faster than the noise component, which tends to dominate high frequencies. This gradient filter therefore allows the removal or attenuation of the noise at the higher frequencies. Our tests of various filters of this kind showed that Elliptically Symmetrical Fourier Filters (ESFF) with a Gaussian-shaped intensity profile are successful at recovering some images affected by the along-track noise structures. These ESFFs work like low-pass filters, suppressing noise by eliminating high frequencies while preserving low frequencies, which represent most of the real image data. Figure 5c shows a graphical representation of such a filter. The use of a Gaussian intensity profile along with the filter provides a sharp frequency cut-off without producing ringing, a fact attributed to the filter's smooth transition between low and high frequencies. If an elliptical filter with an appropriate size and geometry is chosen, horizontal noise situated at extreme high frequencies (i.e., Figure 5b[2], line C_1-C_1') can also be eliminated, avoiding the extensive use of notch filters.

Discussion

The use of both notch and elliptical filters, as described above, can solve all noise problems in the VNIR channels and in SWIR Channel 5. This is because the noise that is within these channels does not coincide with the range of frequencies representing the majority of the image data. There are situations, however, when important noise components fall within the frequency range of data representing the real scene. In other words, the noise energy is mixed with the image energy at the low frequency end of the range. This typically occurs in SWIR Channels 6, 7, and 8, which are severely affected by all sets of interference patterns. Experiments over these images using very small elliptical filters show that noise can be reduced, but at the expense of high-frequency real-image information. This causes the inverted FFT image to look blurred and devoid of useful textural and edge information. Besides, the noise structures are different for each individual SWIR channel and each scene, so a great deal of work is required to design specific filters for each. Because of the Fuyo-1 noise characteristics, the approaches that Rose (1989) and Hummer-Miller (1990) used to remove the noise in AVIRIS and TIMS images, respectively, caused by a few discrete sinusoidal harmonics at frequencies where there is little image signal energy, are not suitable for Fuyo-1 processing.

Vaguely similar noise structures to the ones shown by Fuyo-1 data can be found in AVHRR Channel-3 data. In this case, Wiener filtering techniques seem able to reduce noise with minimum image distortion (Simpson and Yhann, 1994). Although successful, there are several drawbacks on developing such filters. Among them, (1) they are computationally difficult to implement, (2) they require estimates of the magnitude of the noisy channel and the energy spectrum of the noise, and (3) sometimes there are a number of complex assumptions (Full and Epler, 1993).

Zonal Notch Filter

A pair of channels with highly correlated noise structures (at similar frequencies), but with poorly correlated scene information, should provide the means to isolate the systematic defects present in any multichannel data. It follows from this that a very accurate filter, which is scene dependent, can be derived from the difference between these two channels in the frequency domain. From this hypothesis we develop a new method to restore Fuyo-1 images using Fourier operators, as we show that the above condition can usually be satisfied by at least two of the Fuyo-1 channels.

The choice of a pair of channels covering the specifications mentioned above strongly depends upon the individual scene information. However, some general rules can be addressed. It is demonstrable that the spectral information present in Channel -1, -2, -3, and -5 data is variable, but is distinct from that contained in Channels 6, 7, and 8 (as per Figure 2). This means that scene information between these sets is likely to be poorly correlated. We have previously observed that the noise components are much more obtrusive in Channels 6, 7, and 8 than in any of the other channels. The VNIR channels are the least corrupted. Channel 5 is the least affected by additive noise within the SWIR set, but always contains it. Channel 5, consequently, will always rank as a potential candidate to be combined with any of the other individual SWIR channels for the frequency filtering operation.

Assuming, by way of an illustration, that Channel 5 and Channel 8 fulfill the prime conditions stated before, the next step involves transforming both channels to the Fourier domain and extracting their magnitude components. Because many image frequency spectra decrease rather rapidly as a function of increasing frequency, their high frequency terms have a tendency to become obscured when displayed in image form (Gonzalez and Wintz, 1977). We applied a contrast stretch to the magnitude plots to bring out this low-level information, which, if shown simply as a standard Fourier spectrum, is beyond the dynamic range of the display sys-

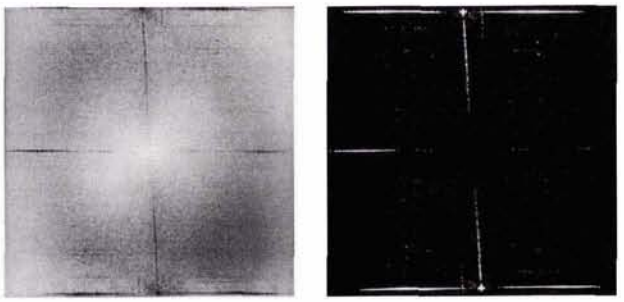

(a) (b)

Figure 6. (a) Difference magnitude image (DMI), resulting from subtracting the magnitude plots of Channels 5 and 8, showing noise (dark) and image components (bright) concentrated at distinct DN values (dark pixels represent "negative" difference and bright pixels represent "positive" difference). (b) Zonal Notch Filter (ZNF) derived from this DMI (in this picture, all of the values representing the estimated noise were mapped to 255 DN and the rest of the image to zero, for greater clarity).

tem. The visual result of such contrast stretch is similar to that of applying the traditional logarithmic re-scaling to the Fourier spectrum (Gonzalez and Wintz, 1977), but has the advantage of being a quicker procedure.

Considering that in both magnitude images (1) the same Gaussian-stretch parameters are applied, (2) the Cartesian position of the worst defects (spots and spikes) approximately coincide, and (3) there is a reasonable difference between the scene information, then the majority of the noise components should be detected and isolated by subtracting the magnitude plot of the channel that shows the noise structures most predominantly from the other. Figure 6a shows the magnitude plot resulting from the difference between Channel 8 (Figure 5b[1]) and Channel 5. It is evident from Figure 5b[1] that there is no apparent separability between the grey levels representing the periodic noise structures from those representing the rest of the image data (e.g., the DN values for the center of the spikes have values close to those at and around the zero frequency point). The difference between the magnitude images (DMI) (Figure 6a), however, shows all the noise components concentrated at low DN values (dark pixels), while the pixels comprising the rest of the image signal remain at much higher DN levels (brighter pixels). The resulting DMI itself, although distinguishing the noise, would be difficult to interpret if transformed back to the spatial domain. However, it can be used as a basis for creating an effective scene-dependent filter. Such a filter can be produced, first, by re-scaling the DMI, produced by the above procedure, to form a byte image. A threshold value is estimated which separates the noise component of the image from that of the real image component more precisely. This threshold is best found using an interactive pseudo-coloring routine to highlight the values representing noise. Once a threshold value which represents the break point between the noise and the real image components is found, a simple linear mapping function can be applied. This function is used to map to zero all of the values in the DMI representing noise, and to map all of the real image data to one, thereby creating a binary mask. Figure 6b illustrates a binary mask created by this procedure (the DN values for noise and image signals were mapped to 255 and 0, respectively, for greater clarity). Such a mask can be termed a "Zonal Notch Filter" (ZNF). Note that all noise components are isolated in the process, including some other minor noise represented by small bright spots away from the main "noise axes." Figure 7 outlines the processing steps involved in creating the ZNF.

Once a ZNF has been created, it is combined multiplicatively with each channel's FFT. This removes the unwanted noise component of the original image, as this is mapped to zero in the frequency domain. Figure 8 shows the processing steps for using this filter to remove noise from an original input image. ZNFs will remove all noise components introduced by both the optical sensor failures and those caused by the pre-processing algorithms, without removing too much of the image information, providing that a suitable break point is chosen. Because the ZNF is a bit image, and because the spatial frequency of the noise is unaffected by stretched or unstretched magnitude plots, the multiplication of a ZNF to either produces identical results as regards noise reduction after the images are transformed back to the spatial domain. However, the use of Gaussian-stretched magnitude brings some special effects to the scene in the spatial domain which can be exploited to minimize another problem within Fuyo-1 data, as we shall see in the following section.

Brightness Saturation

Brightness saturation is another problem within Fuyo-1 imagery. The quantization of OPS data to only six bits (64 radi-

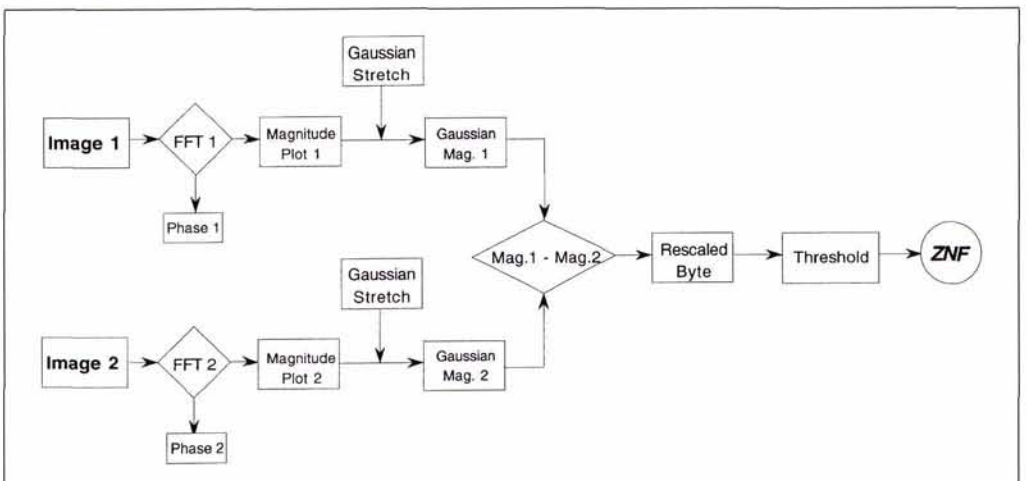

Figure 7. Flow diagram for producing a Zonal Notch Filter from two input channels.

ance levels) means that even scenes containing large differences in luminance and reflectance are recorded as small dynamic ranges of DN. Consequently, details of the image in dark and particularly in very bright regions are not fully represented, as they are usually cut off or saturated (Figure 9). One means to solve such a problem is to use the illumination-reflectance model (see details in Gonzalez and Wintz, 1977) as a basis for a frequency-domain contrast-modifying procedure. Bearing in mind that the illumination component of an image is characterized by gradual spatial variations, but conversely, the reflectance component tends to vary abruptly at junctions of distinct scene attributes, we can assume that they respectively are largely represented by low and high frequencies in the Fourier domain. If this is correct, large patches of bright and dark areas in the scene will appear as low frequencies in the magnitude component of the FFT. In this case, brightness saturation and large-scale shading within an OPS channel can be reduced if the variance of intensities can be equalized by means of a non-linear transformation. This can be achieved by re-distributing the intensity values in the Fourier spectrum into a Gaussian distribution, or, in other words, by simply applying a Gaussian contrast stretch to the spectrum. Because the phase component of the FFT is not affected by this contrast stretch, the angles used to code noise directions are preserved. The result of combining the original phase angle image with the stretched magnitude image yields a non-saturated image in the spatial domain.

Images reconstructed by this method show balanced luminance gradients and more uniform display of local details (compare Figures 3b and 9 with Figure 10 and Figure 3c with Figure 11), with histograms fitting a Gaussian shape. Because the original images tend to show roughly a Gaussian distribution of DN levels, this method does not cause any significant change to the geometry of the histograms, just a shortening or broadening of them depending on the standard deviation used. However, it must be emphasized that, for those pictures whose initial histograms are bi-modal, with crucial information contained in the smaller peak, histogram flattening will probably destroy visual perceptibility of the image. This simple approach may not have the mathematical sophistication of some techniques with similar aims, such as homomorphic filtering (Gonzalez and Wintz, 1977), unsharp masking (Pratt, 1978; Andrews and Hunt 1977), adaptive filtering and histogram equalization (Peli and Lim, 1982; Pizer *et al.*, 1987), local mean and variance (Lee, 1980), balance contrast enhancement (Guo, 1991), and other histogram transformations (Hummel, 1977), but our experimental results indicate it to be a highly effective and elegant tool to simultaneously enhance features in dark or brightly saturated areas of an image, using a minimum of computing time.

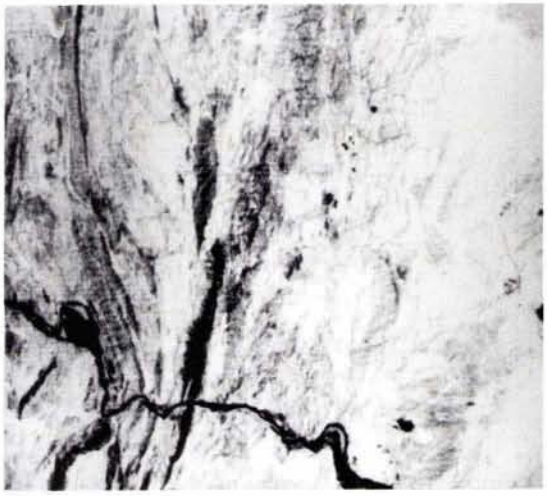

Figure 9. Brightness saturation on original Level-2 OPS Channel 8. Simultaneous observation of geological details in both dark or brightly saturated areas is impossible.

This method can also be performed to produce better false color composites. Soha and Schwartz (1978) demonstrated that band triplets exhibiting low inter-band correlation contain more multispectral information and a wider color variation after appropriate enhancement. However, band triplets with proper contrast and low inter-band correlation may produce poor color composites (due to color bias) if the average brightness of one band is significantly higher or lower than those of the other two bands (Guo, 1991). If the histograms of the three channels can be balanced in such a way that they share the same value range and average brightness, more colorful composites can be obtained (Guo, 1991). The Balance Contrast Enhancement Technique (BCET) (Guo, 1991) proved to be successful in achieving this, being effective in scenes showing both bi-modal and uni-modal histograms. In the same way, the technique used here to equalize frequencies in the Fourier domain can be performed to yield channels with the same mean and value range by setting the spatial frequency distribution of all of the channels to a common Gaussian shape. Fuyo-1 false color composites obtained by this method and finely "tuned" using a simple linear stretch contain a large variation of hue within

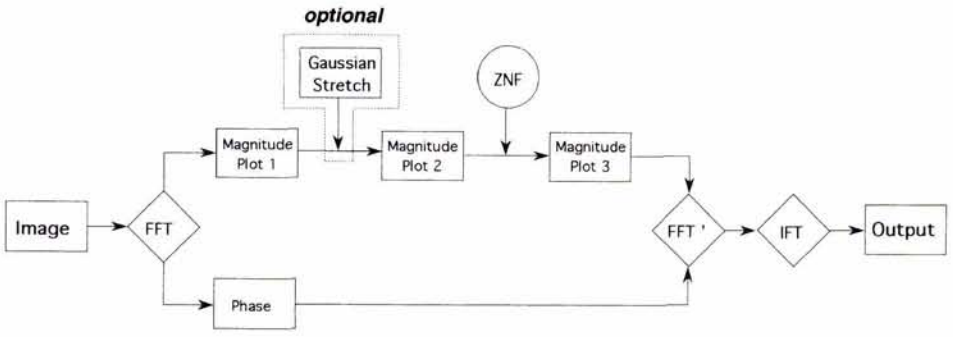

Figure 8. Flow diagram of the steps required for a complete restoration (noise removal and brightness equalization) of a single input channel.

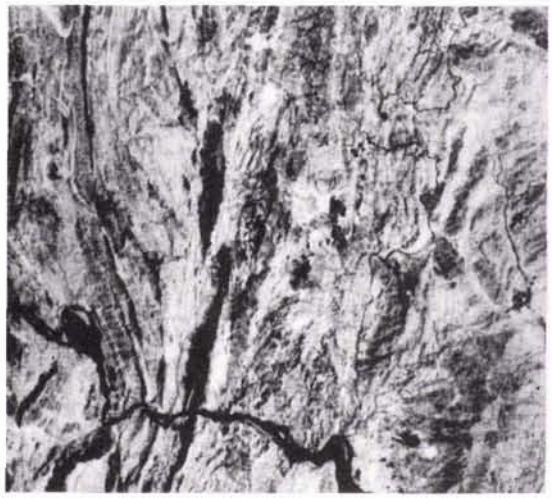

Figure 10. Restored Level-2 Fuyo-1 SWIR OPS Channel 8. Compare with Figure 3b and 9.

intensity and saturation changes. This procedure can be performed as a part of the noise removal technique as illustrated in Figure 8.

Results

Figures 10 and 11 are the combined results of applying a ZNF and the low-frequency equalization technique to the highly corrupted Level-2 OPS images of Channels 8 (Eritrea) and 6 (Oman). The original images (Figures 3b and 3c) contain large amounts of both horizontal and sub-vertical noise structures in the spatial domain (Figure 4b), which represent a variety of complex interference patterns in the frequency domain (Figure 5b). Applying both of these techniques together has removed all of these interference patterns as well as the brightness saturation, and has yielded images showing a significant improvement in quality. All OPS channels filtered by these methods exhibit similar improvements, although achievements over SWIR Channels 6 and 7 may vary according to scene information and original data quality.

Occasionally, problems can arise when trying to remove the noise component of an image which contains strong real linear features (such as topographic ridges due to bedding or deformation fabrics) parallel to the direction of the along-track striping. If such features occur, it may be difficult to distinguish the noise component from the genuine image component in the frequency domain. In such situations, great care has to be taken when determining the threshold value for the ZNF to ensure that important image data is not mistaken as a part of the noise component. If this situation arises, it is best to choose a threshold value which is biased towards leaving a little of the noise component, but does not remove much of the image component.

Images restored by any of the methods described in this paper, despite their good image quality and usefulness in many geological applications, are not recommended for use in quantitative measures of reflectance. The reasons for that vary from technique to technique and with the extent to which they are applied. Although the raw image hues can be well preserved in the whole process, relative brightness components can be modified, compromising any quantitative usage. In cases where quantitative analysis is crucial, it should precede "clean-up" filtering. The same applies for segmentation, enhancement, and classification procedures. For example, techniques such as principal component analysis (PCA), decorrelation-stretch, ratio, and intensity-saturation-hue (ISH) transformation work better if clean-up filtering is performed on the final enhanced/classified images. The noise, which is greatly emphasized by these methods, is just as effectively removed *post hoc*.

Care is also needed when performing the brightness saturation minimization procedure (which can be used as part of the ZNF method). Although it successfully reduces the large patches of saturated areas in the image by equalizing low spatial frequencies, the operation may "wash out" important spectral and tonal differences within these patches. The brightness correction also reduces total image variance. That is simply because there is a decrease in image saturation at the expense of illumination, the component responsible for the overall dynamic range of the scene. Despite these problems, there are situations when brightness saturation can completely avoid the observation of very bright and very dark areas in Fuyo-1 scenes at the same time, so that it must be corrected. In these cases, the best way to avoid arbitrary "loss" of information is to inspect the tonal and spectral differences in the image prior to restoration.

Conclusions

By comparing Figures 3b and 3c to Figures 10 and 11, the benefits of the Zonal Notch Filter described here are evident. This technique, which is simple to implement and efficient, transforms noise-corrupted Fuyo-1 images (Level-0 or Level-2) into useful images containing a minimum of noise structures and with increased dynamic ranges. Color composites of OPS channels filtered by this technique contain a wealth of spectral information as originally anticipated by the system design team. In comparative studies between cleaned Fuyo-1 composites and Landsat Thematic Mapper (TM) composites, Fuyo-1 data have already shown that, despite the initial quality of the Level-2 data, very useful and meaningful geological information can be extracted which is not apparent on TM images (de Souza Filho and Drury, 1994; *Denniss et al.*, 1994).

Whereas a ZNF significantly suppresses the noise in the SWIR data, it does not totally eliminate the noise. This is true for all filtering methods in which the noise and signal overlap in the spatial and spectral domains (Simpson and Yhann, 1994). In these cases, the noise cannot be totally removed

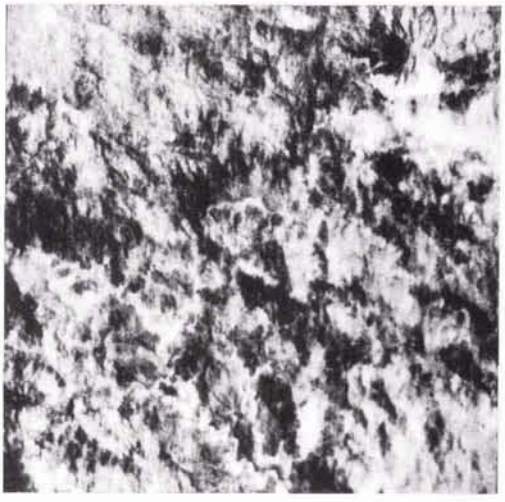

Figure 11. Restored Level-2 Fuyo-1 SWIR OPS Channel 6. Compare with Figure 3c.

without a complete description of the noise or signal. The best that can be achieved is that the residual noise is reduced as much as possible with as little as possible image distortion introduced.

The Fuyo-1 SWIR radiometer ceased operation in December 1993 due to severe malfunction in the cooling system. Since March 1994 just the VNIR radiometer has been operating. However, about 40,000 scenes comprising all seven Fuyo-1 OPS channels were collected throughout the world and are presently available from NASDA's archives. Some 66,000 scenes (about 31,000 with less than 30 percent cloud coverage) were acquired up to October 1994. We enthusiastically foresee that these scenes can now achieve some of their unique potential, particularly in geological applications, if the methodologies presented and introduced in this paper are applied.

Acknowledgments

These results were obtained as a part of the NASDA/MITI JERS-1 verification program (J-0103 Principal Investigator: S. A. Drury, and J-0107 Principal Investigator: D. A. Rothery). De Souza and Denniss are funded by CAPES (Brazil) and SERC (Britain) research studentships, respectively. Takashi Nishidai (ERSDAC) is acknowledged for all his help with JERS-1 data acquisition. Many thanks go to P. Bland, L. Kirstein, B. De Vries, F. Garland, T. Kennedy, W. Rogan, A. Harris, and A. Butterwoth of the "Vicarage Research Centre" for many "discussions." Three anonymous referees suggested many improvements to the original manuscript.

References

Andrews, H.C., and B.R. Hunt, 1977. *Digital Image Restoration*, Prentice Hall, New Jersey, 238 p.

Anonymous, MITI / NASDA Report, 1990. *Outline of the JERS-1 System*, October, 31 p.

Anonymous, Japan Resources Observation System Organization (JAROS) Report, 1991. *JERS-1 Mission Instruments*, June, 8 p.

Castleman, K.R., 1979. *Digital Image Processing*, Prentice Hall, New Jersey, 429 p.

Crippen, R.E., J.P. Ford, and R.G. Blom, 1994. An Evaluation of Fuyo-1 (JERS-1) Optical Data for Geological Interpretation, *Proceedings of the ERIM Tenth Thematic Conference on Geological Remote Sensing*, San Antonio, Texas, 2:606.

de Souza Filho, C.R, and S.A. Drury, 1994. Evaluation of Fuyo-1 (JERS-1) Imagery for Geological Mapping in Arid Terrains, JERS-1 Verification Program Meeting, Tokyo (Abstracts).

Denniss, A.M., D.A. Rothery, G. Ceuleneer, and I. Amri, 1994. Lithological Discrimination Using Landsat and JERS-1 SWIR Data in the Oman Ophiolite, *Proceedings of the Tenth Thematic Conference on Geological Remote Sensing*, San Antonio, Texas, 9-12 May, 2:97–108.

Full, W.E., and D.T. Epler, 1993. Evaluation of Multichannel Wiener Filters Applied to Fine Resolution Passive Microwave Images of First-Year Sea Ice, *Remote Sens. Environ.*, 44:1–23.

Gonzalez, R.C., and P. Wintz, 1977. *Digital Image Processing*, Addison-Wesley, Massachusetts, 502 p.

Grove, C.I., S.J. Hook, and E.D. Paylor II, 1992. *Laboratory Reflectance Spectra of 160 Minerals, 0.4 to 2.5 Micrometers*, JPL-NASA, California.

Guo, L.J., 1991. Balance Contrast Enhancement Technique and Its Application in Image Color Composition, *Int.J.Rem.Sens.*, 12(10): 2133–2151.

Hummel, R., 1977. Image Enhancement by Histogram Transformations, *Computer, Graphics and Image Processing*, 6:184–195.

Hummer-Miller, S., 1990. Techniques for Noise Removal and Registration of TIMS Data, *Photogrammetric Engineering & Remote Sensing*, 56(1):49–53.

Hunt, G.R., 1980. Electromagnetic Radiation: The Communication Link in Remote Sensing, *Remote Sensing in Geology* (B.S. Siegal and A.R. Gillespie, editors), Wiley, New York, pp. 5–45.

———, 1981. Spectra of Kaolin Minerals in Altered Volcanic Rocks, *Clays and Clay Minerals*, 29:76–81.

Hunt, G.R., and R.P. Ashley, 1979. Spectra of Altered Rocks in the Visible and Near Infrared, *Econ. Geol.*, 74:1613–1629.

Hunt, G.R., and J.W. Salisbury, 1970. Visible and Near-Infrared Spectra of Minerals and Rocks: II. Carbonates, *Modern Geology*, 2:23–30.

Jain, A.K., 1989. *Fundamentals of Digital Image Processing*, Prentice-Hall, London, 385 p.

Lee, J., 1980. Digital Image Enhancement and Noise Filtering by Use of Local Statistics, *IEEE Transactions on Pattern Analysis and Machine Intelligence*, PAMI-2(2):165–168.

Marion, A., 1991. *An Introduction to Image Processing*, Chapman and Hall, London, 305 p.

Matsunaga, T., S. Tsuchida, and Y. Yamaguchi, 1993. Processing of JERS-1 OPS SWIR Images of Yerington, Nevada, *Proceedings of the 15th Japanese Conference on Remote Sensing*, pp. 5–7 (in Japanese).

Niblack, W., 1986. *An Introduction to Digital Image Processing*, Prentice-Hall, New Jersey, 316 p.

Nishidai, T., 1993a, Early Results from Japan's Earth Resources Satellite Fuyo-1, *Proceedings of JERS-1 Information Exchange Meeting (Presentation Materials)*, Kogakuin University, Tokyo, Japan, 16-17 August, pp. 49–50.

———, 1993b. Early Results from 'Fuyo-1' Japan's Earth Resources Satellite (JERS-1), *Int. J. Remote Sensing*, 14(9):1825–1833.

Ono, H., 1993. Status of JERS-1 OPS, *Proceedings of JERS-1 Information Exchange Meeting (Presentation Materials)*, Kogakuin University, Tokyo, Japan, 16-17 August, pp. 39–48.

Peli, T., and J.S. Lim, 1982. Adaptive Filtering for Image Enhancement, *Optical Engineering*, 21(1):108–114.

Pizer, S.M., E.P. Amburn, J.D. Austin, R. Cromartie, A. Geselowitz, T. Greer, B.H. Romeny, J.B. Zimmerman, and K. Zuiderveld, 1987. Adaptive Histogram Equalisation and Its Variations, *Computer, Vision, Graphics and Image Processing*, 39:355–368.

Pratt, W.K., 1978. *Digital Image Processing*, Wiley-Interscience, New York, 749 p.

Rose, J.F., 1989. Spatial Interference in the AVIRIS Imaging Spectrometer, *Photogrammetric Engineering & Remote Sensing*, 55(9):1339–1346.

Rothery, D.A., and G.A. Hunt, 1990. A Simple Way to Perform Decorrelation Stretching and Related Techniques on Menu-Driven Processing Systems, *Int. Jour. Rem. Sens*, 1:133–137.

Shimada, M., 1993. Image Quality of SAR/OPS, *Proceedings of JERS-1 Information Exchange Meeting (Presentation Materials)*, Kogakuin University, Tokyo, Japan, 16-17 August, pp. 90–132.

Schowengerdt, R.A., 1983. *Techniques for Image Processing and Classification in Remote Sensing*, Academic Press, London, 245 p.

Simpson, J.J., and S.R. Yhann, 1994. Reduction of Noise in AVHRR Channel 3 Data with Minimum Distortion, *IEEE Transactions on Geoscience and Remote Sensing*, 32(2):315–328.

Soha, J.M., and A.A. Schwartz, 1978. Multispectral Histogram Normalisation Contrast Enhancement, *Proceedings of the 5th Canadian Symposium of Remote Sensing*, Victoria, Canada, August, pp. 86–93.

Tanaka, T., and M. Shimada, 1993. Status of JERS-1 and its Operation, *Proceedings of JERS-1 Information Exchange Meeting (Presentation Materials)*, Kogakuin University, Tokyo, Japan, 16-17 August, pp. 9–27.

Yamaguchi, Y., 1987. Possible Techniques for Lithological Discrimination Using the Short-Wavelength-Infrared Bands of the Japanese ERS-1, *Remote Sensing of Environment*, 23(1):117–129.

———, 1988. Spectral Indices for Vegetation and Rock Type Discrimination Using the Optical Sensor of the Japanese ERS-1, *Proceedings of the Sixth Thematic Conference: Remote Sensing for Exploration Geology*, Houston, Texas, 16-19 May, pp. 159–168.

Yamaguchi, Y., H. Hase, and K. Ogawa, 1992. Remote Sensing for Geothermal Applications, *Episodes*, 15(1):62–67.

(Received 18 August 1994; accepted 25 May 1995; revised 25 July 1995)